Cement & Concrete Composites 48 (2014) 53–66

Contents lists available at ScienceDirect

Cement & Concrete Composites

journal homepage: www.elsevier.com/locate/cemconcomp

Properties of strain hardening ultra high performance fiber reinforced concrete (UHP-FRC) under direct tensile loading

K. Wille [a,*], S. El-Tawil [b], A.E. Naaman [b]

[a] Department of Civil & Environmental Engineering, University of Connecticut, 261 Glenbrook Road Unit 2037, Storrs, CT 06269-3037, USA
[b] Department of Civil & Environmental Engineering, University of Michigan, 2350 Hayward, G.G. Brown, Ann Arbor, MI 48109-2125, USA

ARTICLE INFO

Article history:
Received 1 May 2013
Received in revised form 6 November 2013
Accepted 31 December 2013
Available online 13 January 2014

Keywords:
Ultra-high performance concrete (UHPC)
Ultra high performance fiber reinforced concrete (UHP-FRC)
Strain hardening
Multiple cracking
Strain energy
Tension

ABSTRACT

Enhanced matrix packing density and tailored fiber-to-matrix interface bond properties have led to the recent development of ultra-high performance fiber reinforced concrete (UHP-FRC) with improved material tensile performance in terms of strength, ductility and energy absorption capacity. The objective of this research is to experimentally investigate and analyze the uniaxial tensile behavior of the new material. The paper reviews and categorizes a variety of tensile test setups used by other researchers and presents a revised tensile set up tailored to obtain reliable results with minimal preparation effort. The experimental investigation considers three types of steel fibers, each in three different volume fractions. Elastic, strain hardening and softening tensile parameters, such as first cracking stress and strain, elastic and strain hardening modulus, composite strength and energy dissipation capacity, of the UHP-FRCs are characterized, analyzed and linked to the crack pattern observed by microscopic analysis. Models are proposed for representing the tensile stress–strain response of the material.

1. Introduction

Ultra-high performance concrete (UHPC) is a specially formulated concrete with a compressive strength of 150 MPa or higher. When properly reinforced with steel fibers, the material can be made to fail in a fairly ductile manner in compression (as opposed to brittle explosive modes when unreinforced), exhibit pseudo-ductility in tension, provide exceptional energy absorption prior to fracture, and undergo distributed cracking with extremely small crack widths prior to crack localization.

Ultra-high performance fiber reinforced concrete (UHP-FRC) can be categorized according to the performance classification scheme proposed by Naaman and Reinhardt [1], which places cementitious composites into the following categories of behavior: (Level 1) deflection softening or crack controlling with little enhancement in mechanical properties, (Level 2) deflection hardening, (Level 3) tensile strain hardening and (Level 4) high energy absorbing (see Fig. 1). Fig. 1 include the following parameters: cracking stress σ_{cc} and associated strain ε_{cc}, elastic modulus E_{cc}, composite tensile strength or post-cracking strength σ_{pc}, modulus of rupture σ_{f1} and equivalent bending strength σ_{f2}. It is worth noticing that the stress versus strain relationship is only valid prior to matrix cracking. The material softening behavior is characterized by stress versus crack opening relationship. During the multiple cracking phase, the material can be characterized by stress versus strain values assuming a smeared cracking approach. Further information about calculating fracture energy and crack opening are provided in Wille and Naaman [2]. In Fig. 1 level 0 has been added to the performance classification to illustrate the behavior of non-fiber reinforced concrete as a reference material. The material used in this research aims for the fourth and highest performance level that is both a strain-hardening material and a high energy-absorbing material.

In order to more clearly distinguish between performance levels 3 and 4, the variable, g, defined as the energy absorption capacity prior to tension softening, is introduced as an evaluation parameter (see Fig. 1). Experimental results presented herein and by other researchers suggest that fiber reinforced concrete material with performance level 4 should have a high value of g. Until more data becomes available, a value of $g \geqslant 50$ kJ/m^3 is suggested here to define performance level 4. Record values for g have been reported by Wille et al. [3], such as $g = 304$ kJ/m^3 for Sifcon-UHP-FRC with 5.5% of fiber volume fraction and $g = 128$ kJ/m^3 for a UHP-FRC with only 1% of fiber volume fraction. Jungwirth and Muttoni reported $g = 25$ kJ/m^3 for Ceracem®, a UHP-FRC with 2.5% fiber volume fraction [4]. All investigated UHP-FRCs in this research are characterized by g-values in the range of 55–94 kJ/m^3, and are thus classified as high energy absorbent UHP-FRC material (Level 4) according to the modified classification scheme discussed above.

* Corresponding author. Tel.: +1 860 486 2074.
E-mail address: kwille@engr.uconn.edu (K. Wille).

http://dx.doi.org/10.1016/j.cemconcomp.2013.12.015
0958-9465/

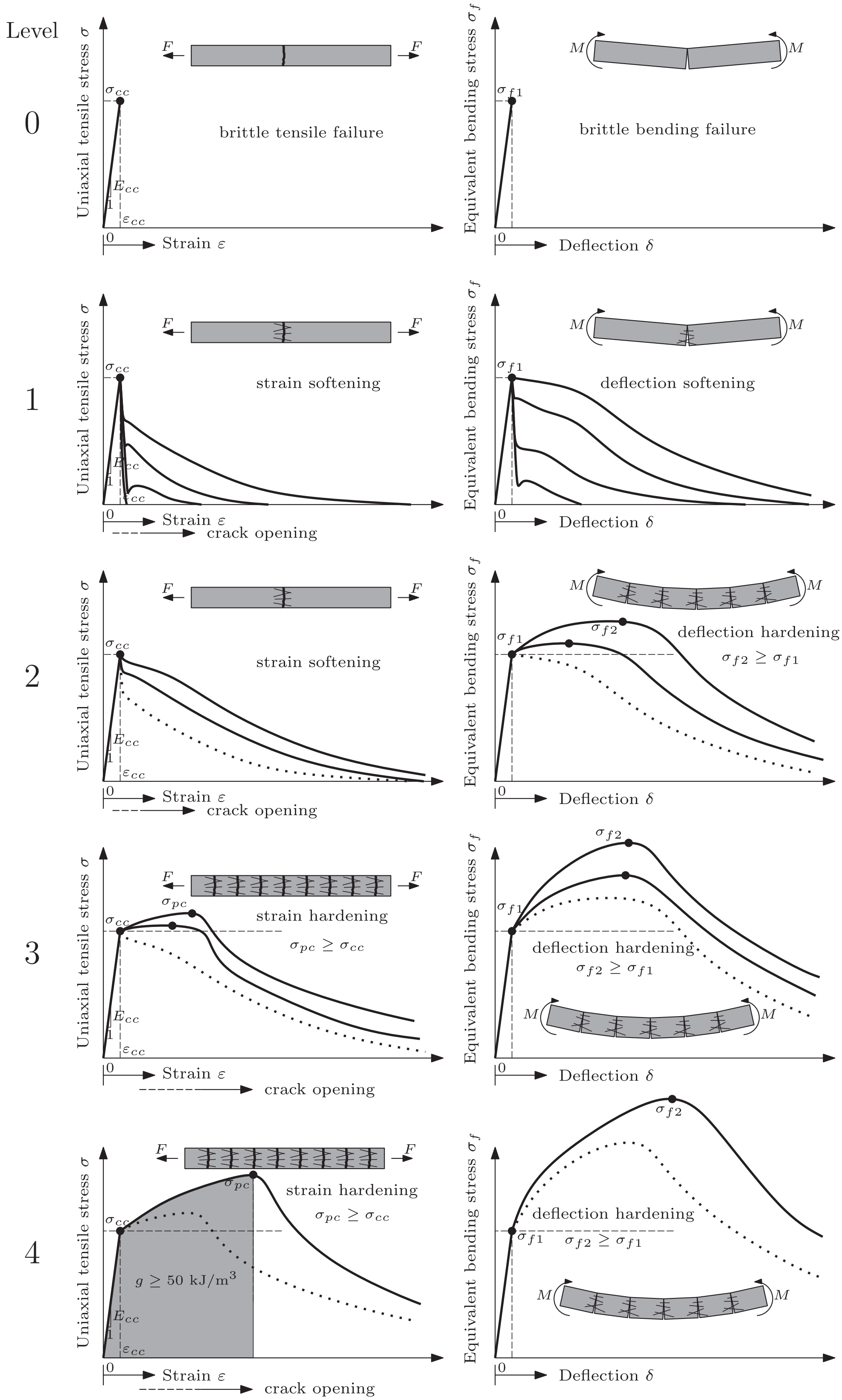

Fig. 1. Illustration and definition of the performance levels of fiber reinforced concrete.

The UHP-FRCs considered herein were developed by applying the ternary approach of fiber reinforced cement composites (Fig. 2) that entailed: 1) optimizing the matrix particle density (Wille et al. [5,6]), 2) using very high strength steel fibers (Wille et al. [3,7]), and 3) tailoring the fiber-to-matrix interface bond properties (Wille and Naaman [8,9]). Previous research has shown that the new material can be tailored to achieve the following mechanical performances under direct tensile loading: (a) post-cracking

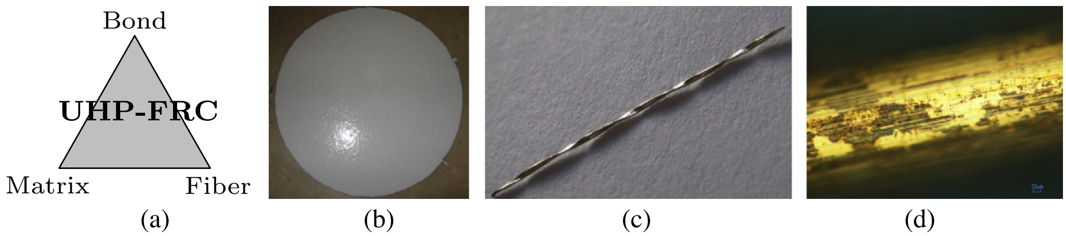

Fig. 2. Material composite design, (a) cementitious composite, (b) matrix, (c) high performance fiber and (d) fiber–matrix-bond.

tensile strengths up to $\sigma_{pc} \approx 37$ MPa (5.4ksi), (b) post-cracking strains up to $\varepsilon_{pc} \approx 1\%$, (c) tensile strengths with 1% of fiber volume fraction up to $\sigma_{pc} \approx 16$ MPa (2.3ksi), (d) energy absorption capacity with 1% of fiber volume fraction up to $g \approx 130$ kJ/m^3, and (e) average crack widths as well as crack spacing as small as 4 µm and 1 mm, respectively [3]. As reported in Wille et al. [3], the documented energy absorption capacity exceeds by at least 5 times the energy values of steel fiber reinforced UHP-FRC reported by other researchers.

The objective of this paper is to enhance understanding of the tensile behavior of newly developed UHP-FRC through documentation and analysis of recent test results. This understanding is necessary in order to better predict the mechanical properties of UHP-FRC and facilitate its potential use in the field.

2. Typical tensile properties of UHP-FRC

Fig. 3 shows the stress strain curve for a typical UHP-FRC material tested in direct tension. Following the definition of Naaman and Reinhardt [1], the material is strain hardening, because its tensile strength, σ_{pc}, is in excess of its cracking stress, σ_{cc}. The idealized modeling approach distinguishes the tensile behavior into three parts (Fig. 3) as follows:

(*Part I*): *strain based elastic part*, determined by the initial tensile behavior up to σ_{cc}, which is defined as a fictitious point of transition from ideal linear elastic to best fitted linear strain-hardening behavior, and determined by the associated strain ε_{cc} and the elastic modulus E_{cc},
(*Part II*): *strain based strain hardening part*, determined by the dissipated energy per unit volume $g_{f,A}$, 99% of the tensile strength of the composite σ_{pc}, its associated strain ε_{pc} and ε_{soft}, hardening modulus E_{hc} and the residual strain ε_{res} and,
(*Part III*): *crack opening based softening part*, which is characterized by the dissipated energy per crack surface area $G_{f,B}$.

In a tensile strain hardening material, Part II is associated with multiple cracking, while Part III pertains to the softening curve associated with crack localization (Fig. 3). The unloading modulus E_{pc} is of importance to clearly distinguish between energy dissipation during strain hardening (volume based) and during softening (area based) (Wille and Naaman [9]).

3. Direct tensile test method

Tensile testing of materials with strain hardening behavior accompanied by multiple cracking is particularly challenging. While AFGC-SETRA [10] and JSCE [11] both provide recommendations on how to perform uniaxial tensile tests on UHP-FRC and HPFRCC materials, there are currently no testing standards available that define the test conditions, specimen geometry, and analytical procedures necessary to fully characterize the tensile properties of strain-hardening cementitious material. Predetermination of crack development by notching the specimen in bending or direct tension is commonly utilized to simplify the test setup, deformation control, measurement system and data analysis. However, doing so may not be appropriate for capturing the strain hardening behavior of UHP-FRC.

In comparison to bending or wedge splitting tests, uniaxial tensile tests directly provide material tensile behavior over all three stages (elastic, strain hardening, softening) without the need of high computational effort for backward calculation of the material tensile response. However, direct tensile tests are challenging to perform. Difficulties in obtaining evenly distributed stresses throughout the cross section and controlling a stable load versus displacement/crack opening response has limited the number of researchers performing direct tensile tests on cementitious materials and composites. Specimen shapes, which can be distinguished into dogbone shape (Table 1), unnotched (Table 2) and notched prisms or cylinders (Table 3), and the type of gripping system (fixed or rotating boundary condition) significantly influence the test results in all three stages of behavior. Some aspects related to specimen shape and boundary conditions have been addressed in [39].

Although top glued unnotched prisms or cylinders of UHP-FRC with strain hardening behavior (performance Level 3) have been

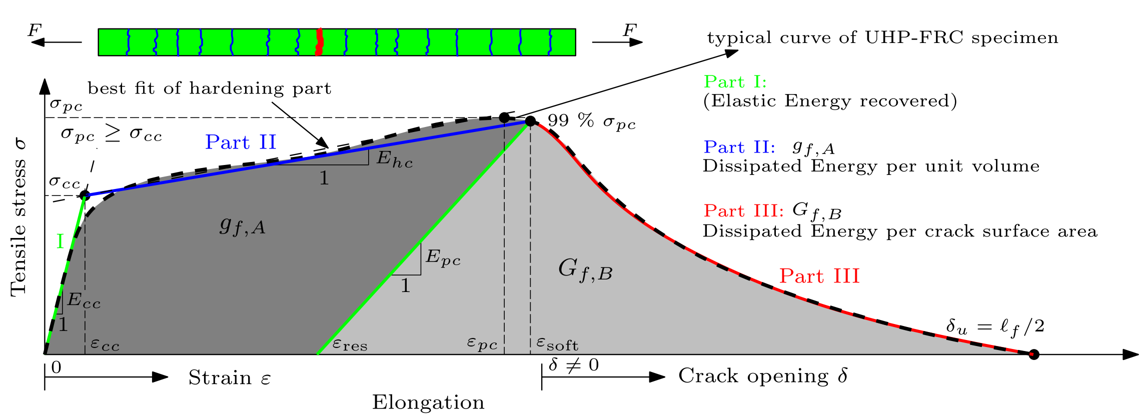

Fig. 3. Strain hardening tensile behavior of UHP-FRC and idealized modeling approach (horizontal axis scale magnified for clarity).

Table 1
Direct tension test setups – dogbone shaped specimens.

Shape dogbone	Material (–)	Performance level (–)	Length, width and depth of constant area (total specimen) in (mm)			Diff. area	Grip/attachment	DOF[a] top–bottom	Ref.
			L	W	D				
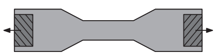	UHP-FRC	4	80 (330)	30 (60)	13 (13)	50%	Fixed	0–0	[12,13]
	HPFRCC	3–4	80 (240)	24 (40)	40 (40)	60%	Fixed	0–0	[14]
	HPFRCC	4	152 (457)	38 (76)	76 (76)	50%	Self-clamping friction grip[b]	1–1	[16]
	HPFRCC	3	150 (200)	25 (40)	25 (25)	63%	Anchored/pinned	1–1	[17]
	HPFRCC	3	200 (525)	50 (125)	13 (13)	40%	Anchored/pinned	1–1	[17]
	UHP-FRC	3–4	178 (525)	51 (125)	25 (25)	41%	Anchored/pinned	1–1	[7]
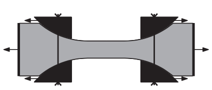	UHP-FRC	3–4	200 (750)	100 (300)	50 (50)	33%	Top glued/anchored	0–0	[18]
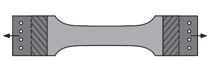	UHP-FRC	3	250 (740)	100 (200)	35 (35)	50%	Side glued/pinned	1–1	[19]
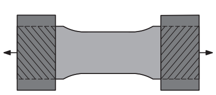	UHP-FRC	3	200 (700)	160 (200)	45 (45)	80%	Side glued + anchored (greased)	0–0	[3]
	HPFRCC	3–4	80 (330)	30 (60)	13/30 (13/30)	50%	Clamped/fixed/pinned	0/2–0/2	[11]
	Plain concrete	0	200 (400)	60 (100)	100 (100)	60%	Top glued	0–0	[20]
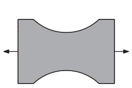	Plain concrete	0	0[c] (150)[c]	60[c] (100)[c]	100[c] (100)[c]	60%	Top glued/pinned	2–2	[21]
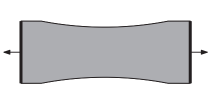	Plain lightweight concrete	0	0 (270)	80[d] (100)[d]	–	64%	Top glued/fixed	0–0	[22]

[a] DOF – degree of freedom.
[b] Similar to Saito and Imai [15].
[c] Other sizes were also investigated.
[d] Diameter of the cylinder.

investigated in tension [33,35], this test setup is primarily useful in determining the elastic behavior prior to cracking. However, it is not appropriate for capturing strain hardening behavior. When applied to strain hardening UHP-FRC, this setup generally results in bond failure due to the limited matrix tensile strength [33]. Side-glued unnotched prisms have been successfully used to obtain strain hardening tensile behavior [31,32]. However, it is important to note that the measurement length should ideally remain away from the ends to avoid the constraints introduced by the support system. Notched specimens have been designed to investigate the softening behavior of plain and fiber reinforced concrete (performance Level 0–2). Notched specimens are not suitable for characterizing elastic or strain hardening tensile behavior. Crack predetermination and sudden change in cross-section results in stress localization and earlier crack initiation. Moreover, the small height of the notch does not allow the development of multiple cracks or investigation of crack spacing.

In order to capture strain hardening behavior (performance Level 3–4) a variety of dogbone shaped specimens have been successfully used in the past (Table 1). They all have the following general characteristics: (a) a middle part with constant or nearly constant area to promote multiple cracking behavior, (b) larger cross sectional areas at the supports to avoid support failure, and (c) smooth transition from the supported area to the middle part to reduce the

Table 2
Direct tension test setups – unnotched prism/cylinder specimens.

Shape unnotched prism/cylinder	Material (–)	Performance level (–)	Length, width and depth of constant area (total specimen) in (mm)			Diff. area	Grip/attachment	DOF[a] top–bottom	Ref.
			L	W	D				
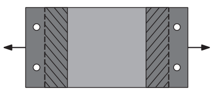	FRC	<3	127 (330)	127 (127)	28 (28)	100%	Side glued/pinned	0–0	[23]
	FRC/ECC	3/4	205 (305)	76 (76)	13 (13)	100%	Side glued/pinned	0–0	[24,25]
	UHP-FRC	3	102 (432)	51 (51)	51 (51)	100%	Side glued + clamped /fixed	0–0	[26]
	UHP-FRC	3	160 (160)	70 (70)	70 (70)	100%	Top glued	0–0	[27]
	Plain concrete/UHP-FRC	0/3	200 (200)	100[b] (100)[b]	–	100%	op glued	0–0	[28,29]

[a] DOF – degree of freedom.
[b] Diameter of the cylinder.

Table 3
Direct tension test setups – notched prism/cylinder specimens.

Shape notched prism/cylinder	Material (–)	Performance level (–)	Length, width and depth of constant area (total specimen) in (mm)			Diff. area	Grip/attachment	DOF[a] top–bottom	Ref.
			L	W	D				
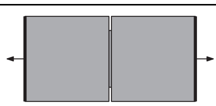	FRC	<3	2 (152)	51 (76)	51 (76)	44%	Top glued	0–0	[30]
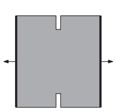	FRC	<3	3 (55)	42 (60)	50 (50)	70%	Top glued	0–0	[31]
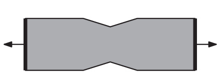	FRC	2	1 (254)	51 (76)	13 (13)	67%	Top glued	0–0	[32]
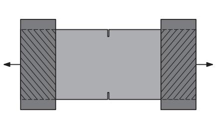	UHP-FRC	3–4	~5 (500)	160 (200)	50 (50)	80%	Side glued + anchored (greased)	0–0	[33,34]
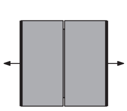	FRC/UHP-FRC	2/3	2–5 (150)	135[a] (150)[b]	–	81%	Top glued	0–0	[29,35–37]
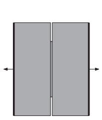	UHP-FRC	3–4	2 (60)	44[b] (74)[b]	–	35%	Top glued	0–0	[38]

[a] DOF – degree of freedom.
[b] Diameter of the cylinder.

effects of stress concentrations. The specimens are glued, anchored or clamped to the machine and the attachment is either fixed or pinned.

In addition to Tables 1–3 summarize test setups and specimen geometries of prisms or cylinders, which are tested unnotched or notched, respectively. In Tables 1–3 the performance level of the tested materials is in agreement with Fig. 1, "Diff. Area" provides the percentile of test area to area of load applied and "DOF" signifies the degree of freedom at the top and bottom of the specimen. A designation of "0" means all translations and rotations are constrained, "1" means rotation around one axis is not constrained and "2" means rotations about two axes are not constrained.

The summary of test setups and specimen geometries shows the wide range of variation in direct tensile testing and the lack of a standardized method. Each research group referred to in Tables 1–3 used a specific geometry and attachment based on preparation effort, material type including largest material constituent and emphasis of material characterization, e.g. long constant areas allow the investigation of multiple cracking and average crack spacing, notched specimens facilitate the investigation of the material softening (stress versus crack opening behavior). Pinned end conditions facilitate specimen alignment and even stress distribution prior to cracking, but do not support an even crack opening throughout the cross section in comparison to a fixed boundary condition. In order to capture strain-hardening behavior, the fiber bridging forces beyond matrix cracking strength need to be transferred into the attachment. Therefore, top-glued specimens without increased cross-sectional area at the end are not suitable for investigating strain-hardening behavior.

Based on AASHTO T 132-87 [40] and the tensile test setup in [17] a direct tensile test setup has been used (as shown in Fig. 4) to fulfill the following requirements, i.e. it (a) accommodates small specimens so as to reduce material usage, (b) employs specimens that are easy to cast, prepare, install (no glue) and align (anchored/rotational boundary condition), (c) uses specimens with a region of constant area to capture multiple cracking, (d) employs specimens that do not suffer head or bond failure and do not require a haunch or head reinforcement, (e) employs an easy and quickly deployable, removable, lightweight (to permit future high strain rate tests, i.e. has small inertia) and reusable measurement system with high accuracy, (f) has a high probability of achieving uniaxial stress (achieved through manual alignment – translation free in two directions and automatic alignment – free in rotation around two axes), and (g) facilitates stable and even crack growth throughout the cross section.

It is suggested that the largest material constituent should be limited to one fifth of the smallest specimen size that is 5 mm. This permits testing paste and mortar like materials, such as the UHPC used in this research, which has a maximum grain size of 0.8 mm. In comparison to the length of the fibers (13–30 mm), the height and width (25/25 mm) of the specimen molds are deemed small. This leads to fiber alignment in the direction of the applied tensile load, which is further enhanced by pouring the specimens in layers.

4. Materials and preparations

As indicated previously, the authors have developed [5,6] successful ultra-high performance concrete mixtures (UHPC). The key advantages of the new UHPC are that it can be made using components commercially available on the US market, and achieves at least 200 MPa compressive strength without special curing regimes that involve heat treatment or pressure. These advantages significantly facilitate on-site application, potentially promoting wide spread use of the material in industrial applications. In addition to the above advantages, the UHP-FRCs can be designed to be very flowable, exhibiting self-consolidating properties, such that no vibration is needed to cast them. More information about flowability and fiber agglomeration of UHP-FRCs is given in [41]. The mix proportion, average strengths of UHPC and an UHP-FRC example are given in Table 4. By replacing the equivalent volume of sand with steel fibers (properties described in Table 5) nine different self-consolidating UHP-FRCs were prepared and their tensile behavior investigated as shown in Table 6. In Tables 5 and 6, S indicates smooth straight steel fibers, T indicates twisted steel fibers and H indicates end hooked steel fibers.

In accordance with [7], the UHP-FRCs are poured in layers in dogbone shaped specimens to full capacity, but without any vibration. After casting, the specimens are covered and stored at room temperature for 24 h. Afterward they are removed from their molds and stored in a water tank at 20 °C for additional 25 days. All specimens are then tested at 28 days. About 48 h prior to testing the specimens are removed from water and left to dry in the laboratory environment. About 24 h prior to testing, a spray coating is applied on the surface of the middle portion of each specimen for better crack detection.

On the day of testing, each specimen is carefully installed into the test setup. A small pretension is applied and the specimen is manually moved slightly into the best aligned position. Before starting the test, each specimen is preloaded up to 40% and unloaded down to 5% of the matrix cracking strength. This is repeated 3 times to further improve the specimen alignment without crack initiation. The loading speed is set to 0.01 mm/s (0.025 in/min), which results in an estimated strain rate of $\dot{\varepsilon} = 0.00013$ 1/s. Three to six specimens are tested from each series. Each test is analyzed

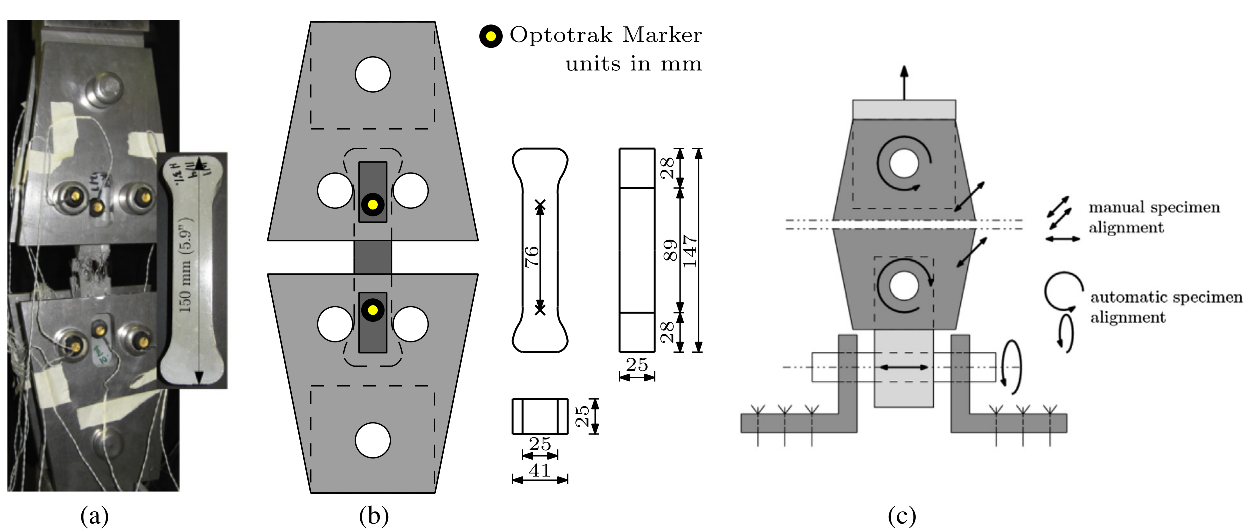

Fig. 4. Direct tensile test setup used in this research, (a) test (b), specimen geometry and fixture and (c) grip system and its degree of freedoms.

Table 4
Mixtures proportions by weight.

Type	UHPC	UHP-FRC
Cement	1.00	1.00
Silica Fume	0.25	0.25
Glass Powder[a]	0.25	0.25
Water	0.19	0.19
Superplasticizer[b]	0.011	0.011
Sand A[c]	0.31	0.28
Sand B[d]	0.72	0.64
Fiber[e]	0.00	0.27
Fiber in Vol.%	0	3.0
f'_c [*cube*, 28*d*] (MPa)	230	250
f_t [*tension*] (MPa)	7.4–8.5[*]	18

[a] Median particles size 1.7 µm.
[b] Solid content.
[c] Max. grain size 0.2 mm (1/128 in.).
[d] Max. grain size 0.8 mm (1/32 in.).
[e] Straight steel fiber, length/diameter = 13 mm/0.20 mm.
[*] At first cracking, followed by immediate failure.

Table 5
Properties of high strength steel fibers used in this study.

Notation	Form	d_f (mm)	ℓ_f (mm)	ℓ_f/d_f	Tensile strength MPa (ksi)
S	Straight (S)	0.20	13	65	≈2600 (377)
H	Hooked (H)	0.38	30	79	≈2900 (420)
T	Twisted (T)	0.30[a]	18	60	≈2100 (304)

[a] Manufactured out of round wire with d_f = 0.30 mm, shaped into prism a/b = 0.24/0.30 mm.

Table 6
UHP-FRC test series investigated in this study.

Type of fiber	Volume fraction			
	1.5	2.0	2.5	3.0
S	–	X	X	X
H	X	X	–	X
T	X	X	–	X

as discussed next to obtain pertinent tensile parameters, which are then averaged within each series.

5. Analysis of tensile test data

The following identification is defined to facilitate discussion: U stands for UHP-FRC, S, H, T stands for the type of fiber as previously mentioned and the last number represents the fiber volume fraction, e.g. U-T-3 is an ultra-high performance concrete reinforced with 3% per volume of twisted fibers. As an example, Fig. 5a shows the stress versus strain relationship of all five specimens of series U-T-3. The same trend in tensile response (that is, linear elasticity, linear strain hardening followed by nonlinear softening), is observed for all UHP-FRC specimens investigated in this research. As shown in Fig. 3, each tensile test curve is idealized into 3 distinct parts, which results in the parameters σ_{cc}, σ_{pc}, ε_{cc}, ε_{pc}, ε_{res}, E_{cc}, E_{hc}, E_{pc}, g, $g_{f,A}$, $G_{f,B}$ (also see Fig. 5b). The elastic modulus E_{cc} is determined by the slope of the tensile curve prior to matrix cracking. The point σ_{cc} and ε_{cc} are defined by the interception of the elastic line and the line of best fit of strain-hardening part. It is important to point out that, in this case, σ_{cc} does not represent the first cracking stress, per se. Rather, it should be seen as the turning point between elasticity and strain hardening. The strain hardening modulus E_{hc} is then determined by the slope between σ_{cc} and 0.99% of the composite tensile strength σ_{pc} with the associated strain values of ε_{cc} and ε_{soft} respectively. The unloading modulus is determined by the reversal point and the point of interception (Fig. 5b) [9]. Strain ε_{pc} and ε_{soft} represent the strain at peak stress and the beginning of softening, respectively.

Whereas *g* represents the energy absorption capacity prior to softening (including the elastic energy), $g_{f,A}$ is determined as the dissipated energy during strain hardening and $G_{f,B}$ as the dissipated energy during softening [9]. The term $G_{f,B}$ is same as the fracture energy G_f, which is defined as the amount of dissipated work needed to generate a unit crack with two completely separated crack surfaces, that is, $G_f = G_{f,B}$.

Once each of the parameters listed above are computed, each specimen can then be characterized by a bi-linear tensile curve up to softening, as shown in Fig. 5b. These curves are averaged within the same series in terms of stress and strain values (Fig. 5c) to facilitate comparison among different series. In addition, each specimen is investigated in terms of crack spacing s_{cr}, defined as the average value of number of cracks per 25 mm, as counted on all four sides of each specimen. This investigation is performed with stereo-microscopic support after unloading, because of the limited crack width, which ranged between 5 and 20 µm. The parameter s_{cr} allowed the calculation of the residual crack opening δ_{pc}.

Figs. 6–8 show the tensile stress versus strain behavior of all investigated specimens. The calculated bi-linear stress-versus strain curve, averaged over all specimens in one series, is plotted on top of the experimental data for comparison. In order to facilitate comparison of the modeled tensile behavior between different series, Fig. 9 summarizes the averaged curves including unloading behavior.

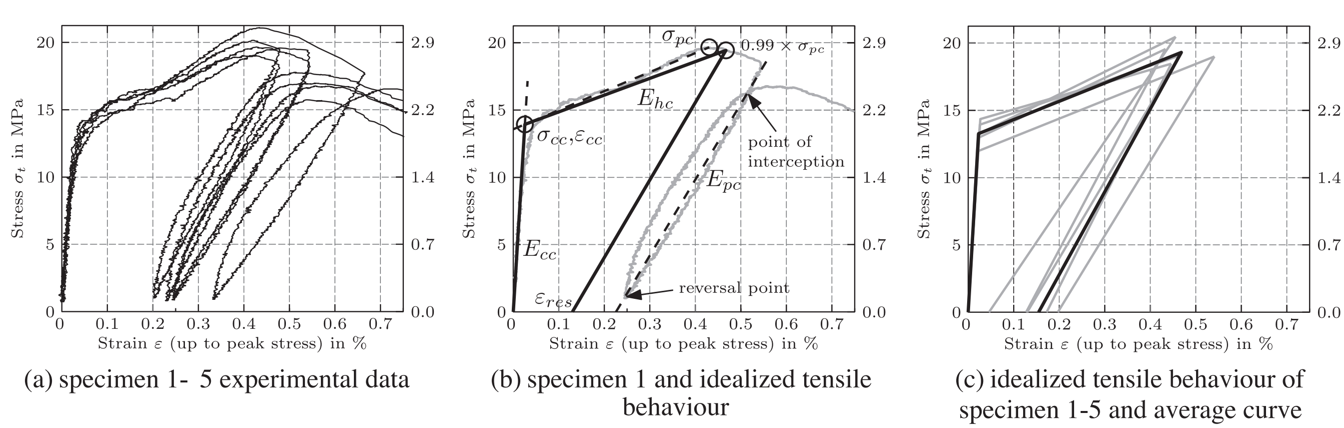

Fig. 5. Analytical procedure for the example of series U-T-3.

6. Results and discussion

6.1. Part I: Elastic regime

The tensile response of the composites in Part I is defined by E_{cc} and σ_{cc}. Fig. 10a and Table 7 summarize the elastic modulus E_{cc} averaged for each UHP-FRC series varied by fiber and fiber volume fraction.

E_{cc} is directly affected by the elastic modulus of the concrete E_c, the elastic modulus of the fibers E_s and the fiber volume fraction V_f. An upper bound of E_{cc} could be predicted as a first approximation from Eq. (1):

$$E_{cc} = (1 - V_f)E_c + V_f E_s \tag{1}$$

where the elastic modulus of the matrix can be estimated from:

$$E_c = k_0 \times f_c^{1/3} \tag{2}$$

Based on the experimental results obtained for E_{cc}, the parameter k_0 was determined by best fit to be k_0 = 9150, assuming values of plain concrete compressive strength of f_c = 230 MPa and elastic modulus of the steel fibers of E_s = 210, 000 MPa. The k_0 value under tensile loading prior to cracking is similar to the k_0 value under compressive loading, and both are dependent on the type of aggregates used in UHP-FRC; they are in the range of k_0 = 8800–11,000 [10,42]. Fig. 10a illustrates the dependency of the composite elastic modulus on the fiber volume fraction and suggests that the type of steel fiber (S, H or T) has no substantial influence on the elastic modulus.

Due to the assumed bi-linear tensile behavior up to initiation of softening, σ_{cc} is defined as a fictitious point of transition from ideal linear elastic to linear strain-hardening behavior. The results of σ_{cc}, averaged for each UHP-FRC series and varied by fiber type and fiber volume fraction, are given in Fig. 10b and are compared to the calculated composite first cracking stress $\sigma_{cc,cal}$:

$$\sigma_{cc,cal} = \sigma_{ct} + \alpha\tau V_f \frac{\ell}{d_f} \tag{3}$$

where σ_{ct} = 7.5 MPa is the assigned matrix tensile strength, selected based on previous experience, $\frac{\ell}{d_f}$ is the fiber slenderness, and $\alpha\tau$ is a product containing the influence of fiber group effect, fiber orientation and bond behavior before cracking (including adhesive component in addition to friction). Fig. 10b shows that σ_{cc} increases with increase of fiber volume fraction for all fiber types. Additionally Fig. 10b shows a comparison between the experimental obtained data and the calculated strength based on Eq. (3). Hereby the product $\alpha\tau$ has been selected to be 0.01, 0.03 and 0.025 for H-, S- and T- fibers, respectively, to fit the data best. Based on the experimental data a best fit curve has been derived and shown as solid curve in Fig. 10b, for simple practical use.

$$\sigma_{cc,fit} = -(V_f - 4)^2 + 14 \tag{4}$$

6.2. Part II: Strain hardening regime

All UHP-FRC investigated in this work exhibited strain-hardening behavior accompanied by multiple cracking. Fig. 11a and Table 7 summarize the averaged composite tensile strength σ_{pc}, which ranges from about 10 MPa at V_f = 1.5% to 20 MPa at V_f = 3% Strong fiber volume dependency ($\sigma_{pc} = -0.9V_f^2 + 9V_f$) and fiber type insensitivity is observed. Previous results have shown [7,9,43,44] that H- and T-fiber outperform S- fibers. The reason for the fiber insensitivity in this research is supported by the high

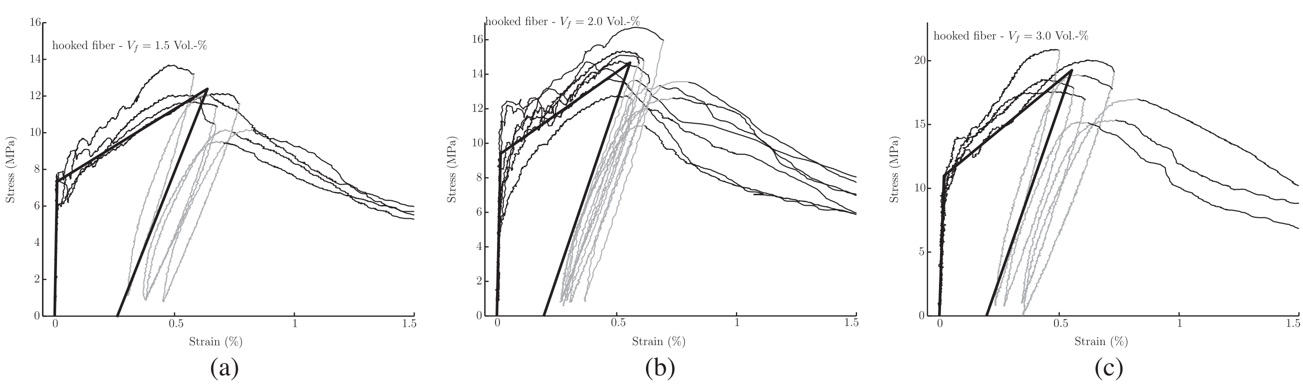

Fig. 6. Test data for U-H-specimens and bi-linear model including unloading line, (a) U-H-15 (b) U-H-2 and (c) U-H-3.

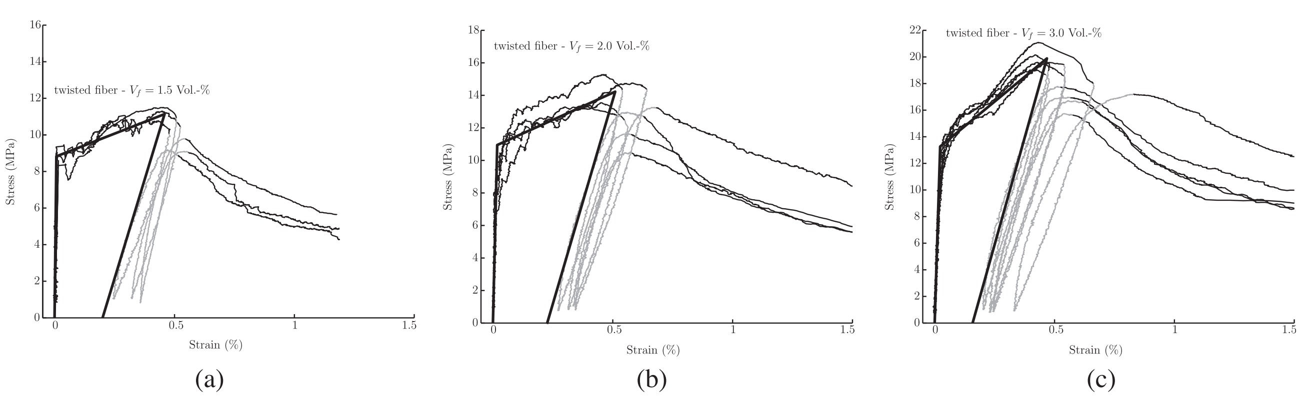

Fig. 7. Test data for U-T-specimens and bi-linear model including unloading line, (a) U-T-15, (b) U-T-2 and (c) U-T-3.

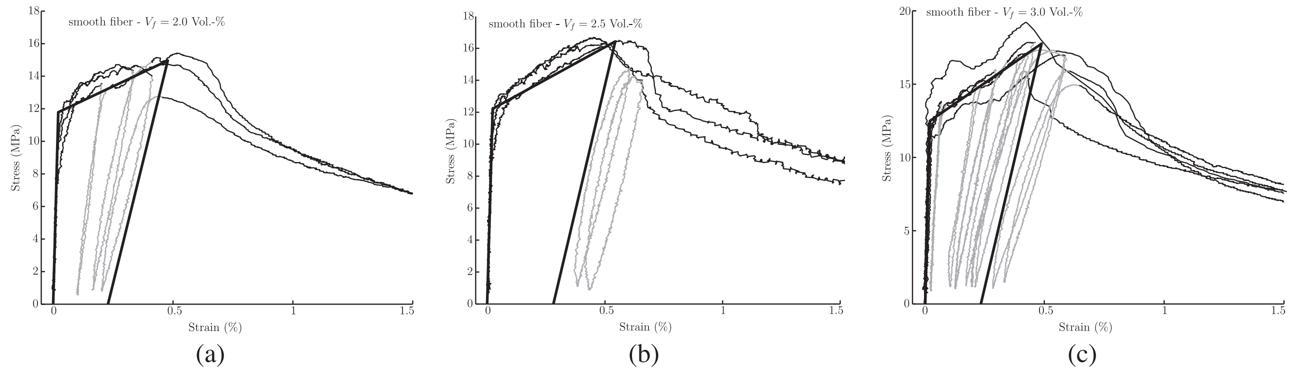

Fig. 8. Test data for U-S-specimens and bi-linear model including unloading line, (a) U-S-2, (b) U-S-25 and (c) U-S-3.

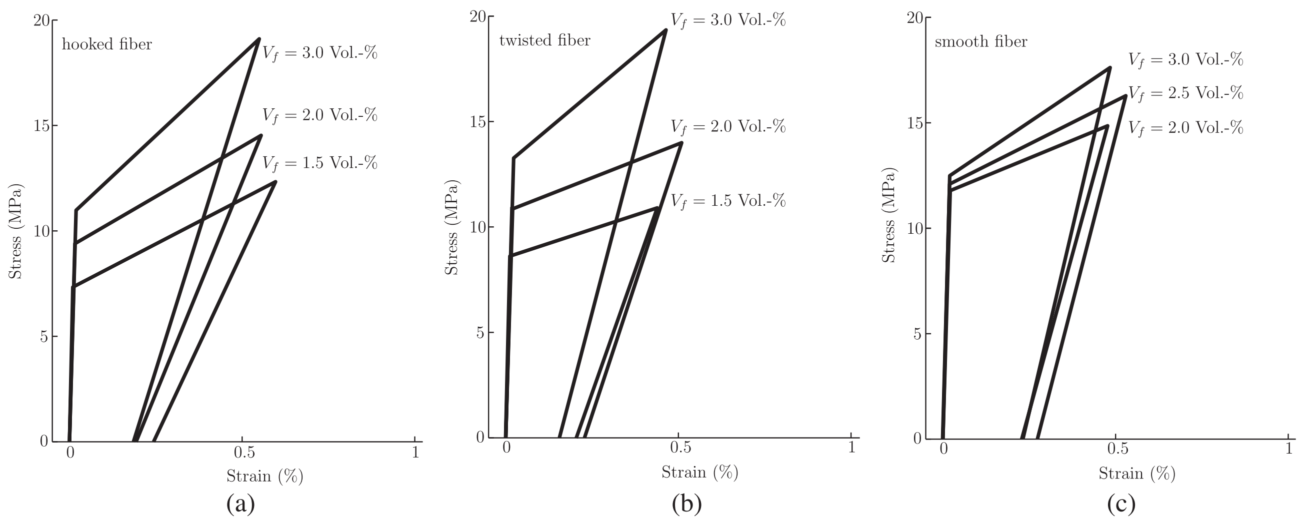

Fig. 9. Comparison of bi-linear models for all series including unloading line, (a) series U-H, (b) series U-T and (c) series U-S.

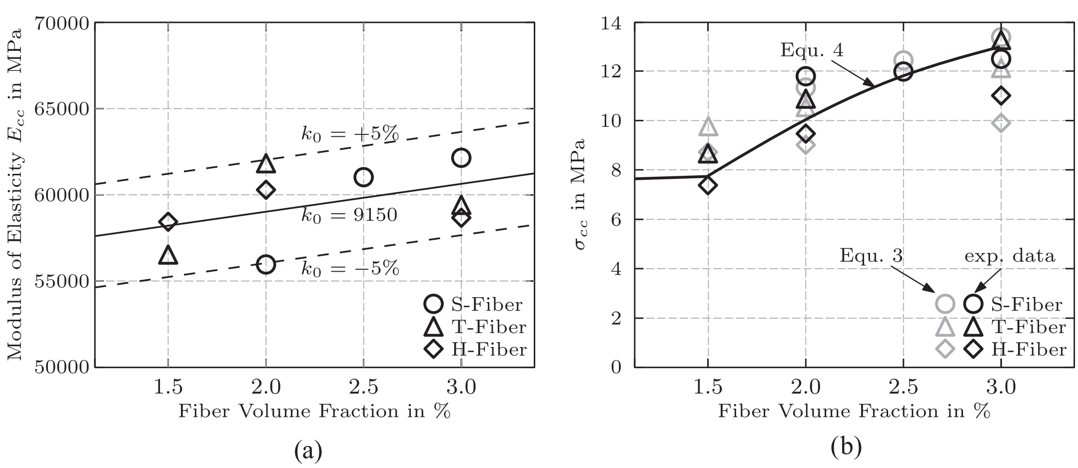

Fig. 10. Elastic tensile parameters of UHP-FRC with different fiber type and volume fraction, (a) E_{cc} averaged for each series and (b) σ_{cc} averaged for each series.

bond strength between S-fiber and optimized UHPC matrix. Similar fiber insensitivity has been found by Rossi [45].

Naaman [46] suggested Eq. (5) to predict the value of σ_{pc}:

$$\sigma_{pc} = \lambda \times \tau \times \frac{\ell_f}{d_f} V_f \tag{5}$$

where τ is the equivalent bond strength between fiber and matrix, ℓ_f/d_f is the fiber aspect ratio and λ is a parameter that accounts for the group effect, averaged embedded length, fiber orientation and spalling effect during pull out of largely inclined fibers. In this research, λ mainly represents the effect of average embedded length and the group effect. The orientation effect is not significantly different between the series of different fiber types due to the preferred alignment of the fibers. λ can be calculated by solving Eq. (5) using the given values of d_f and ℓ_f/d_f (Table 5), V_f and σ_{pc} (Table 7) and τ (Table 8). The value τ represents the equivalent bond strength

Table 7
Test results averaged for each UHP-FRC series.

Notation	V_f (%)	E_{cc} (MPa)	σ_{cc} (MPa)	σ_{pc} (MPa)	λ (–)	σ_{fpc} (MPa)	E_{hc} (MPa) model	E_{hc} (MPa) exp.	ε_{pc} (%)	ε_{soft} (%)	g (kJ/m^3)	s_{cr} (mm)	E_{pc} (MPa)	G_f (kJ/m^2)	δ_{pc} (μm)
U-S-2	2.0	56,000	11.8	15.0	0.96	831	665	883	0.39	0.48	67.0	4.6	5930	22.1	10.6
U-S-2.5	2.5	61,000	12.0	16.5	0.85	733	830	1003	0.47	0.53	76.8	4.2	6330	23.0	11.4
U-S-3	3.0	62,200	12.5	17.8	0.76	658	1090	1250	0.45	0.49	80.0	3.2	6930	25.6	7.5
U-H-1.5	1.5	58,500	7.3	12.4	0.59	918	847	1055	0.49	0.60	65.5	8.1	3480	19.6	20.0
U-H-2	2.0	60,290	9.4	14.7	0.53	815	947	1136	0.48	0.56	73.5	5.8	3970	21.8	11.2
U-H-3	3.0	58,670	11.0	19.3	0.46	713	1526	2113	0.42	0.55	94.1	4.6	5250	30.2	8.6
U-T-1.5	1.5	56,500	8.7	11.1	0.61	820	530	550	0.38	0.44	55.2	4.4	4490	14.0	8.6
U-T-2	2.0	61,750	10.9	14.2	0.59	790	641	788	0.44	0.51	68.8	4.0	4900	19.5	8.9
U-T-3	3.0	59,250	13.3	19.6	0.54	725	1364	1613	0.41	0.47	85.1	3.0	6170	25.3	4.7

averaged over the different fiber embedment lengths L_E in the composite ranging $0 \leqslant L_E \leqslant \ell_f/2$. The values of τ have been calculated based on the average bond strength values τ_{av} of single fiber pull out test at $L_E \approx 6.5$ mm [43] and considering the contribution of frictional and mechanical bond of each fiber [43] as well as possible fiber failure in the case of excessive fiber embedment.

The computed λ values are summarized in Fig. 11b and Table 7. It can be seen that a lower value of λ, and thus a higher reduction in the tensile strength of the composite, occurs in H- and T-fibers. One possible reason for this reduction is the presence of mechanical bond, which causes stress concentration and subsequent local matrix failures that exacerbate adverse inter-fiber interactions. In particular, values of $\lambda \approx 0.6$ at relative low volume fractions of 1.5% suggest that the mechanical bond of the used H- and T-fiber might be too strong to effectively utilize the fiber material as single reinforcement. Fig. 11b also shows that increasing the fiber volume fraction leads to a decrease in λ.

The maximum fiber tensile stress σ_{fpc} at σ_{pc} averaged across all fibers at the failure section indicates the degree of utilization of fiber material (Fig. 12 and Table 7). σ_{fpc} is calculated by Eq. (6) as follows:

$$\sigma_{fpc} = \sigma_{pc}/\phi \times V_f \tag{6}$$

where ϕ is a factor that accounts for fiber orientation, determined to be 0.9 for all series based on an investigation of each specimen's fracture surfaces. The number is quite high because most of the fibers are aligned in the load direction due to the casting method, as previously alluded to. Fig. 12 shows that σ_{fpc} decreases with increase in fiber volume fraction and may be approximated as $\sigma_{fpc} = -100 \times V_f + 1000$ (in MPa). The decrease in σ_{fpc} with increasing fiber volume fraction might be mainly attributed to the fiber group effect. The fiber type insensitivity for σ_{fpc} is similar to the insensitivity of the composite strength σ_{pc} shown in Fig. 11a. This is in contrast to single fiber pull out behavior, where H- and T- fibers reached about twice the σ_{fpc} of S- fibers [9].

The slope of the stress–strain relationship between σ_{cc} and $0.99 \times \sigma_{pc}$ at ε_{soft} is defined as the strain-hardening modulus E_{hc}. The values of E_{hc} averaged over each series show a strong dependency on fiber volume fraction (Fig. 13, Table 7). Three equations are given in Fig. 13 to quantify this dependency. Note that E_{hc} is set to 0 at a volume fraction of 1% according to Fig. 11a, in which $V_f \approx 1\%$ can be seen as the critical volume fraction, $V_{f,crit}$, of fibers used in this research to obtain strain hardening tensile behavior. The reason for selecting $V_{f,crit} = 1\%$ is discussed later on in the paper.

The increase in E_{hc} with increase in V_f is attributed to the development of higher crack bridging forces. Fig. 14 and Table 7 summarize the strain values of each UHPC-series at the composite tensile strength, expressed by ε_{pc}, and at softening, expressed by ε_{soft}. In comparison to Wille et al. [7], slightly higher strain values for U-H have been achieved, which is attributed to the use of higher matrix compressive strength in this work. However, the trend where these strains are independent of fiber volume fraction for U-H occurs herein. U-T and -S show an increase of strain capacity with increase of fiber volume fraction up to $V_f = 2\%$ and 2.5% respectively, as was also observed in [7]. However, further increase in fiber volume fraction up to $V_f = 3\%$ did not lead to additional increase in strain capacity, which is attributed to an increased fiber group effects and crack stabilization.The energy absorption capacity, g, is shown in Fig. 15a. The trends in Fig. 15a can be approximated by the empirical equation $g[\mathrm{kJ/m^3}] = -5V_f^2 + 44V_f$, for $V_f \geqslant V_{f,crit}$. For $V_f < V_{f,crit}$, g will be defined only by the relatively small elastically stored energy. The values of g obtained in this

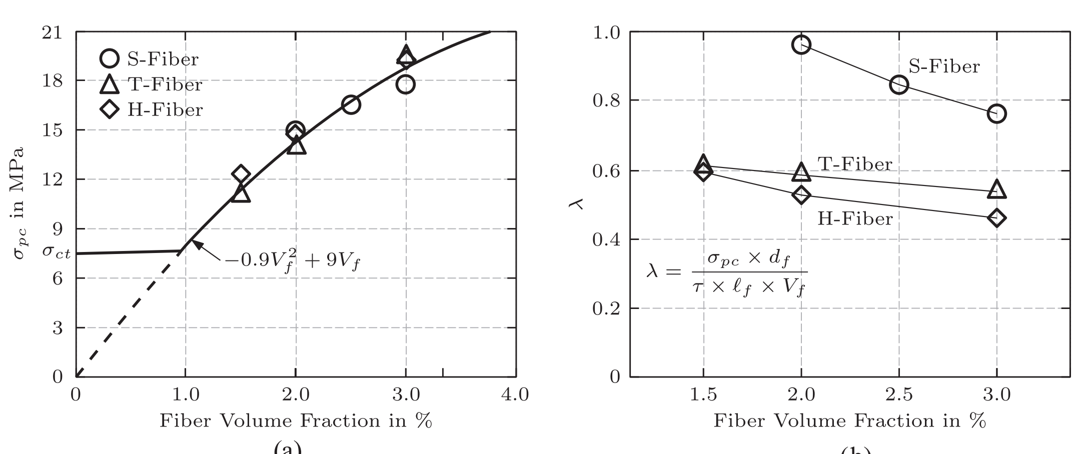

Fig. 11. Composite tensile strengths of U-S, U-T, U-H and fiber type dependent parameter λ, (a) composite tensile strength σ_{pc} and (b) values of λ indicating the group reduction effect.

Table 8
Shear stress values based on single fiber pull out tests.

Notation	τ_{av} MPa (ksi)	τ MPa (ksi)
UHP-FRC-S	8.7–14.2 (1.26–2.06)	12 (1.7)
UHP-FRC-H	42.4 (6.14)	17.6 (2.6)
UHP-FRC-T	24.8 (3.59)	20.1 (2.9)

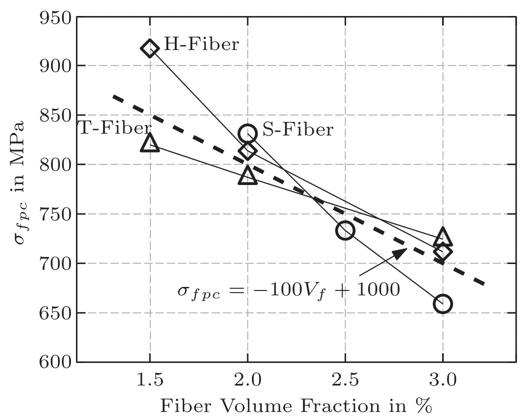

Fig. 12. Fiber stress at σ_{pc} of all investigated UHP-FRC series.

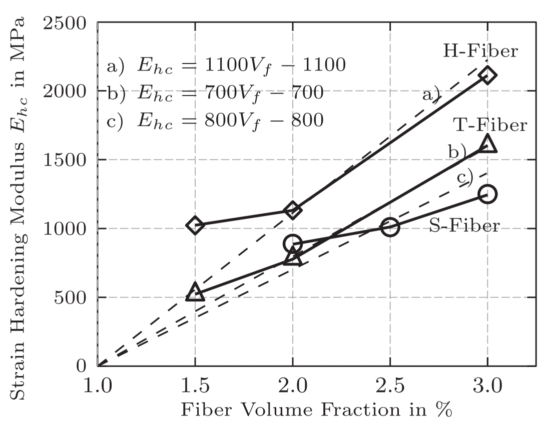

Fig. 13. Strain hardening modulus E_{hc}.

research range from 55 to 94 kJ/m^3, which is about three time the value of Ceracem® (g = 25 kJ/m^3) [4], a comparable UHP-FRC with V_f = 2.5%.

Each specimen was also investigated in terms of crack spacing s_{cr}. The average crack spacing for each series is shown in Fig. 15b and summarized in Table 7. It can be seen that increase in V_f results in a decrease in s_{cr}. The observed linear trend is quantified by the three equations in Fig. 15b. With the given values of s_{cr}, ε_{soft}, σ_{pc} and E_{pc} the average residual crack openings δ_{pc} were calculated by using Eq. (7) [9]. Table 7 shows that the values of δ_{pc} are in the range of 5–20 μm.

$$\delta_{pc} = \left(\varepsilon_{pc} - \frac{0.99\sigma_{pc}}{E_{pc}}\right) \times s_{cr} \tag{7}$$

Fantilli et al. [47] proposed an analytical model to predict the average crack spacing of strain hardening fiber reinforced concrete based on cohesive interface analysis. This model was used herein and its parameters were adjusted to calculate the transmission length ℓ_{tr} and to fit the results of crack spacing s_{cr} for the different UHP-FRCs investigated in this research. The transmission length is defined as the length from the crack face to the point, where no slip between fiber and matrix and thus perfect bond is present.

The following equations have been used [47]:

$$\ell_{tr} \leqslant s_{cr} \leqslant 2\ell_{tr} \tag{8}$$

$$\ell_{tr} = -\frac{\ln\frac{\beta-1}{\beta+1}}{\sqrt{\alpha}} \tag{9}$$

$$\beta = \frac{p_f k_b V_f}{2A_f k_c \sqrt{\alpha}} \tag{10}$$

$$\alpha = \frac{p_f k_b}{A_f}\left(\frac{1}{E_s} + \frac{V_f}{E_c}\right) \tag{11}$$

where p_f is the single fiber perimeter, A_f is the fiber cross sectional area, k_c is the descending slope, defined by $k_c = \frac{f_{ct}}{w_c}$, according to the linear stress-crack opening relationship of UHP-FRC matrix (UHPC) [48] and k_b is the bond parameter, fitted to the experimental data. In order to take the effect of finer orientation into account the fiber volume fraction is corrected by the orientation factor ϕ = 0.9 to $V_{f,cor} = \phi V_f$. The following values were assigned to represent all series considered herein: f_{ct} = 7.5 MPa, w_c = 0.012 mm [48], k_c = 625 MPa/mm, E_c = 56,000 MPa and E_s = 210000 MPa. Table 9 summarizes the assigned parameters and the calculated results.

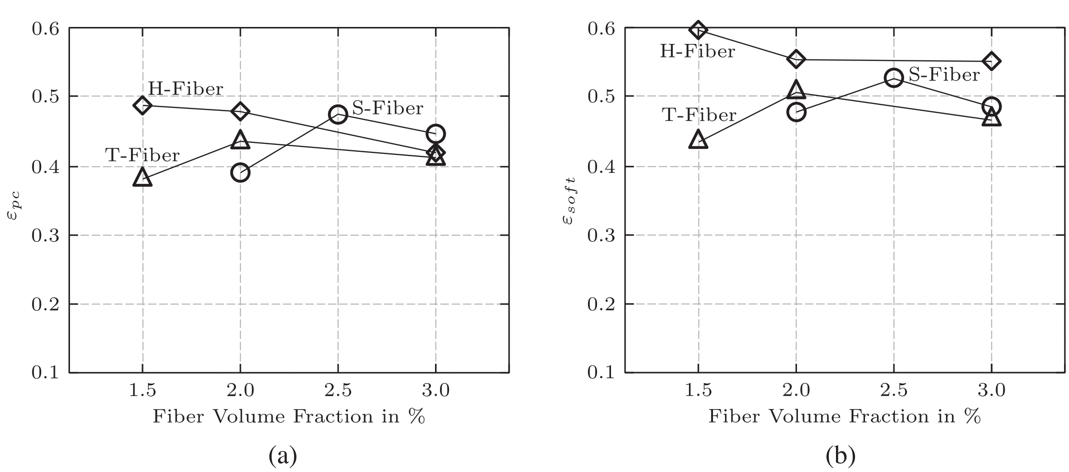

Fig. 14. Strain values at composite tensile strength and at softening, (a) strain at composite tensile strength, ε_{pc} and (b) strain at softening, ε_{soft}.

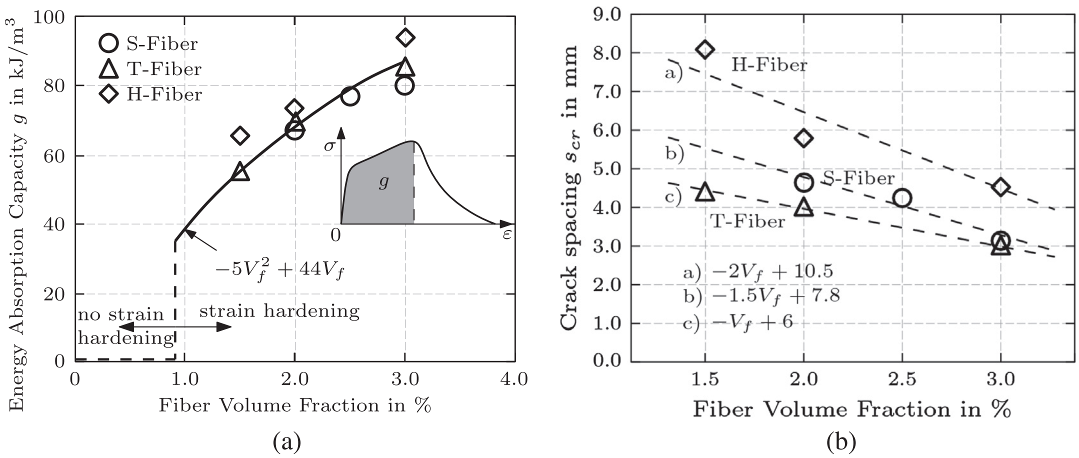

Fig. 15. Energy absorption capacity prior softening g and crack spacing s_{cr}, (a) energy absorption capacity and (b) crack spacing.

Table 9
Model parameter and predicted average crack spacing for each UHP-FRC series.

Notation	V_f (%)	$V_{f,cor}$ (%)	p_f (mm)	A_f (mm^2)	k_b (MPa/mm)	α (1/mm^2)	β (1/mm^2)	ℓ_{tr} (mm)	$2\ell_{tr}$ (mm)	s_{cr} (mm)
U-S-2	2.0	1.80	0.63	0.031	2550	0.259	1.44	3.4	6.7	4.6
U-S-2.5	2.5	2.25	0.63	0.031	2550	0.263	1.79	2.5	4.9	4.2
U-S-3	3.0	2.70	0.63	0.031	2550	0.267	2.13	2.0	3.9	3.2
U-H-1.5	1.5	1.35	1.19	0.113	5000	0.263	1.11	5.8	11.6	8.1
U-H-2	2.0	1.80	1.19	0.113	5000	0.268	1.47	3.2	6.5	5.8
U-H-3	3.0	2.70	1.19	0.113	5000	0.276	2.16	1.9	3.8	4.6
U-T-1.5	1.5	1.35	0.94	0.071	5450	0.364	1.30	3.4	6.7	4.4
U-T-2	2.0	1.80	0.94	0.071	5450	0.369	1.72	2.2	4.4	4.0
U-T-3	3.0	2.70	0.94	0.071	5450	0.381	2.54	1.4	2.7	3.0

By best fitting the numerical and experimental values, k_b is calculated to be $k_b = 2550$ MPa/mm for U-S, $k_b = 5000$ MPa/mm for U-H and $k_b = 5450$ MPa/mm for U-T. The values on the same order of $k_b = 3500$ MPa/mm and $k_b = 4300$ MPa/mm obtained for high strength FRC-H and FRC-T, respectively [47]. The critical fiber volume fraction $V_{f,crit}$ to obtain strain hardening behavior is computed to satisfy the condition of $\beta = 1$ as suggested in [47], which led to $V_{f,crit} \approx 1\%$ for all three types of UHP-FRC. This is in agreement with Fig. 11a. The comparison between analytical and experimental results of crack spacing is show in Fig. 16.

6.3. Part III: Softening regime

As shown in Fig. 3, Part III pertains to the softening part of the stress–strain diagram and corresponds to the fracture energy G_f. In order to account for the effect of the elastically stored energy during softening [2], the unloading modulus E_{pc} was determined for each specimen. Fig. 17a and Table 7 summarize the values of E_{pc}. At comparable fiber volume fractions, specimens with S-fibers achieved higher values than specimens with T- and H- fibers. It is surmised that this may be linked to the higher local stress concentrations that occur in specimens with H- and T-fibers and the corresponding matrix damage that occurs. The values of E_{pc} are comparable to the values obtained in [2] and show a strong fiber volume dependency. Using the computed values of E_{pc}, the fracture energy G_f is calculated for each specimen and averaged for each UHP-FRC series as shown in Fig. 17b and Table 7. Fig. 17b shows that G_f is mainly influenced by the fiber volume fraction and can be quantified by the empirical equation $G_f[\text{kJ/m}^2] = -1.4V_f^2 + 13V_f$. The values of G_f ranges from about 14 to 30 kJ/m^2. These are comparable to reported values of UHP-FRC, i.e. 20 kJ/m^2

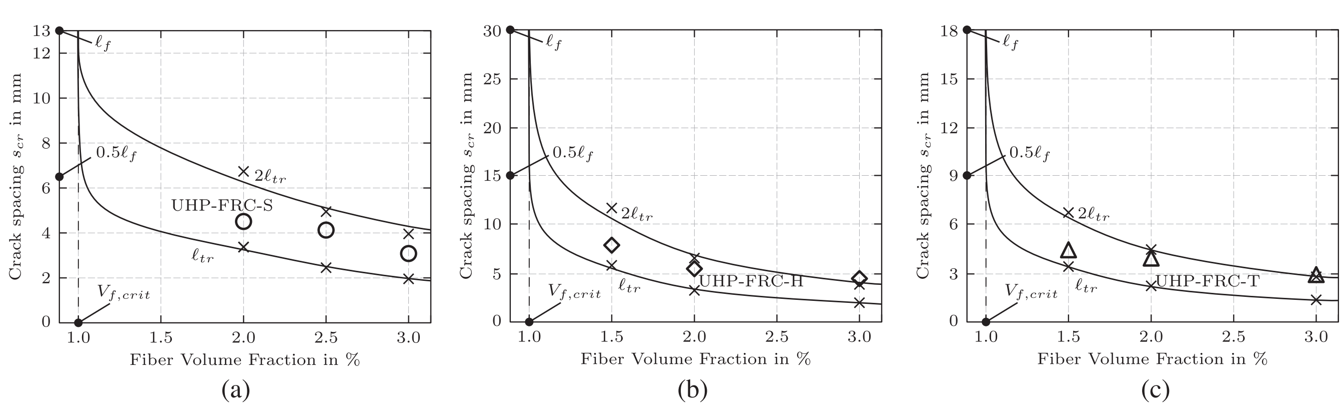

Fig. 16. Comparison of analytical and experimental results of crack spacing, (a) U-S, (b) U-H and (c) U-T.

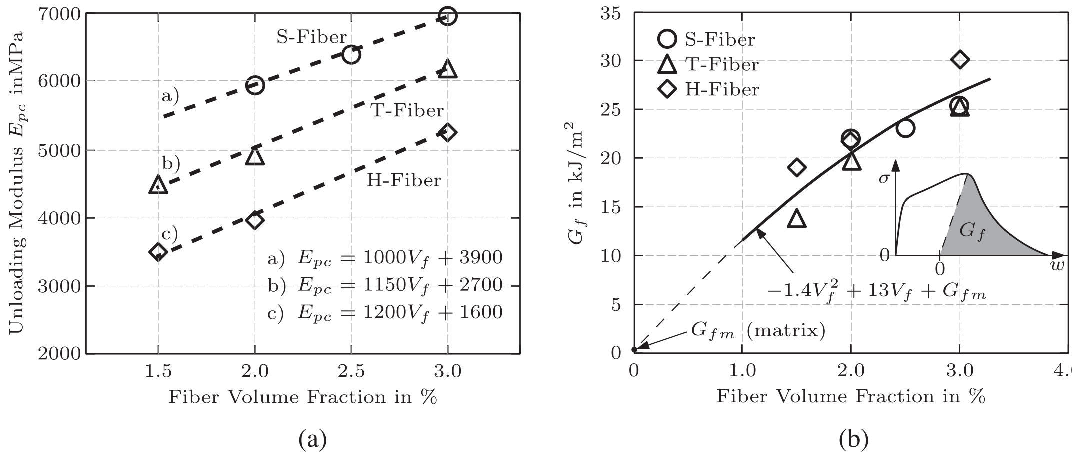

Fig. 17. Test results of unloading modulus and fracture energy, (a) Epc (unloading modulus) and (b) fracture energy.

(V_f = 2.5%) in [49], 20 kJ/m^2 (V_f = 6%) in [19], 24 kJ/m^2 (V_f = 6%) in [50] and 25 kJ/m^2 (V_f = 12%) in [51].

7. Conclusion

Previous research by the authors has shown that ultra-high performance fiber reinforced concrete (UHP-FRC) can be designed to achieve strain hardening with high ductility under direct tensile loading accompanied by high energy absorption capacity. Based on a classification with four performance levels, this type of strain hardening and high energy absorbent concrete is classified as level 4, characterized by strain-hardening behavior and an energy absorption capacity up to peak load in excess of $g \geqslant 50$ kJ/m^3. Until additional data becomes available, this level of performance is suggested based on previous and current research results.

The direct tensile behavior of nine different UHP-FRCs of performance level 4 (varied by fiber type and fiber volume fraction) was experimentally investigated. The analyzed experimental results show, as expected, a strong dependency on fiber volume fraction. Although the three types of fibers, smooth, hooked and twisted, were chosen to cover a wide range of different bond behavior and mechanisms between fiber and matrix, the analyzed results show small differences in terms of tensile strength, strain at peak strength and energy absorption capacity. It is hypothesized that this behavior stems from fiber group effect in the composite and the surprisingly high bond strength observed between smooth fibers and the designed ultra-high strength matrix, which allows development of high tensile stress in the smooth fiber. The higher material utilization of smooth fibers mitigates, in part, the necessity for the additional mechanical bond, present in the hooked and twisted fibers. It is, however, possible that these results may be substantially different if larger specimens were used or if the tests were conducted at high strain rates.

Several equations, obtained either empirically or from simple mechanics were provided to mathematically describe the tensile properties of the tested strain hardening high energy absorbent UHP-FRC. Additionally the experimentally observed crack spacing, which at peak load ranged from 3 to 8 mm, was further analyzed based on the work of Fantilli et al. [47]. Crack spacing, unloading modulus, tensile strength and strain at peak strength were used to calculate the average residual crack openings, which was predicted to range from 5 to 20 μm.

The authors hope that the results and conclusions presented in this study motivate other researchers to further investigate the tensile properties of UHP-FRC, especially using larger size specimens, in order to facilitate the tailoring of their properties for specific practical applications. The high ductility and energy absorbing capacity of the material also imply that is particularly promising for high strain rate applications, such as blast and impact.

Acknowledgements

This work was supported by a fellowship within the Postdoctoral-Programme of the German Academic Exchange Service (DAAD). The second and third writers would also like to acknowledge the support of the University of Michigan and that of the National Science Foundation under grants CMMI 0754505 and 0928193. The writers also like to acknowledge the following companies for providing free material: BASF Construction Chemicals, Bekaert, Chryso Inc., Holcim (US) Inc., Elkem Materials, Grace Construction Products, Lehigh Cement Company, Sika Corporation. The opinions expressed in this paper are those of the writers and do not necessarily reflect the views of the sponsors.

References

[1] Naaman AE, Reinhardt HW. Setting the stage: toward performance based classification of FRC composites. In: Proceedings of 4th RILEM symposium on high performance fiber reinforced cement, composites (HPFRCC4); 2003. p. 1–4.
[2] Wille K, Naaman AE. Fracture energy of UHPFRC under direct tensile loading. In: Jeju Oh BH, editor. Proceedings of FraMCos-7. Fracture mechanics of concrete and concrete structures, Korea. May 23–28, 2010.
[3] Wille K, Naaman AE, El-Tawil S. Ultra high performance fiber reinforced concrete (UHP-FRC) record performance under tensile loading. ACI Concr Int J 2011;33(9):35–41.
[4] Jungwirth J. Muttoni A. Structural behavior of tension members in UHPC. In: Fehling E, Schmidt M, Geisenhanslueke C, editors. Proceedings of international symposium on ultra high performance concrete, Kassel, 2004. p. 533–44.
[5] Wille K, Naaman AE, Parra-Montesinos G. Ultra high performance concrete with compressive strength exceeding 150 MPa (22ksi): A simpler way. ACI Mater J 2011;108(1):46–54.
[6] Wille K, Naaman AE, El-Tawil S, Parra-Montesinos GJ. Ultra-high performance concrete and fiber reinforced concrete: achieving strength and ductility without heat treatment. Mater Struct 2012;45(3):309–24 [published online Aug. 27th 2011].
[7] Wille K, Kim D, Naaman AE. Strain-hardening UHP-FRC with low fiber contents. Mater Struct 2011;44(3):12 [published online Aug. 4th 2010].
[8] Wille K, Naaman AE. Bond Stress Slip Hardening Behavior of Steel Fibers Embedded in Ultra High Performance Concrete. In: Mechtcherine V, Kaliske M, editors. Proceedings of 18th European conference on fracture and damage of advanced fiber-reinforced cement-based materials, contribution to ECF 18. Dresden: Aedificatio Publishers; 2010. p. 99–111.
[9] Wille K, Naaman AE. Pull-out behavior of high strength steel fibers embedded in ultra-high-performance concrete. ACI Mater J 2012;109(4):479–88.
[10] Association Francaise de Genie Civil (AFGC) – Service d'etudes techniques des routes et autoroutes (SETRA), Bétons fibrés à ultra-hautes performances – ultra high performance fibre-reinforced concretes, recommandations provisoires – Interim recommendations; January 2002. p. 153.
[11] Japan Society of Civil Engineers (JSCE). Recommendations for design and construction of high performance fiber reinforced cement composites with multiple fine cracks (HPFRCC); March 2008. p. 113.

[12] Kamal A, Kunieda M, Naoshi U, Nakamura H. Evaluation of crack opening performance of a repair material with strain hardening behavior. Cement Concr Compos 2008;30:863–71.
[13] Kunieda M, Kozawa K, Ueda N, Nakamura H. Fracture analysis of strain hardening cementitious composites by means of discrete modeling of short fibers. In: Jeju Oh BH, editor Proceedings of FraMCos-7. Fracture mechanics of concrete and concrete structures, Korea. May 23–28, 2010. p. 501–8.
[14] Jun P, Mechtcherine V. Behavior of strain-hardening cement-based composites (SHCC) under monotonic and cyclic tensile loading, Part 1 – experimental investigations. Cement Concr Compos 2010;32:801–9.
[15] Saito M, Imai S. Direct tensile fatigue of concrete by the use of friction grips. ACI J 1983(September–October):431–8.
[16] Naaman AE, Homrich JR. Tensile stress strain properties of SIFCON. ACI Mater J 1989;86(3):244–51.
[17] Sujiravorakul C. Development of high performance fiber reinforced cement composites using twisted polygonal steel fibers. Ph.D. dissertation. University of Michigan. Ann, Arbor, 2002. p. 230.
[18] Boulay C, Rossi P, Tailhan JL, Uniaxial tensile test on a new cement composite having a hardening behaviour. In: Proceedings of the sixth international rilem symposium fiber reinforced concretes – BEFIB 2004. Varenna. Italy, September 2004. p. 61–8.
[19] Benson SDP, Karihaloo BL. CARDIFRC – Development and mechanical properties. Part III: uniaxial tensile response and other mechanical properties. Mag Concr Res 2005;57(8):433–43.
[20] Malarics V, Mueller HS. Evaluation of the splitting tension test for concrete from a fracture mechanical point of view. In: Jeju Oh BH, editor. Proceedings of FraMCos-7. Fracture mechanics of concrete and concrete structures, Korea. May 23–28. 2010. p. 709–16.
[21] Van Vliet MRA. Size effect in tensile fracture of concrete and rock. Ph.D. Thesis. Delft University of Technology; 2000.
[22] Wille K, Dehn F, Tue VT, Bruchmechanische Kenngrößen hochfester Leichtbetone. Bauingenieur. Vol. 80. German, June 2005. p. 327–33.
[23] Li Z, Kulkarni SM, Shah SP. New test method for obtaining softening response of unnotched concrete specimen under uniaxial tension. Exp Mech 1993;33:181–8.
[24] Li VC, Wu HC, Maalej M, Mishra DK. Tensile behavior of cement-based composites with random discontinuous steel fibers. J Am Ceram Soc 1996;79(1):74–8. January.
[25] Li V. Engineered Cementitious Composites (ECC) – tailored composites through micromechanical modeling. In: Banthia N, editor. Fiber reinforced concrete: present and future, Canadian Society of Civil Engineers; 1997. 213 p.
[26] Graybeal BA, Baby F, Marchand P, Toutlemonde F. Direct and flexural tension test methods for determination of the tensile stress-strain response of UHPFRC. In: Schmidt M, Fehling E, editors. Proceedings of hipermat 2012, 3rd international symposium on UHPC and nanotechnology for high performance construction materials, Kassel, Germany, March 7–9, 2012, p. 395–402.
[27] Chanvillard G, Rigaud S. Complete Characterisation of tensile properties of DUCTAL® UHP-FRC according to the French recommendations. In: Fourth International workshop on high performance fiber reinforced cement, composites (HPFRCC4); 2003. p. 21–34.
[28] USBR 4914. Procedure for direct tensile strength, static modulus of elasticity, and poisson's ratio of cylindrical concrete specimens in tension. United States Department of Interior. Bureau of Reclamation; 1992.
[29] Graybeal BA. Material property characterization of ultra-high performance concrete. Report No: FHWA-HRT-06-103. August 2006. 188 p.
[30] Wang Y, Li VC, Backer S. Experimental determination of tensile behavior of fiber reinforced concrete. ACI Mater J 1990;87(5):461–8. September–October.
[31] Zhang J, Stang H, Li V. Experimental study on crack bridging in FRC under uniaxial fatigue tension. J Mater Civ Eng ASCE 2000;12(1):66–73.
[32] Roth MJ, Eamon CD, Slawson TR, Tonyan TD, Dubey A. Ultra-high-strength glass fiber-reinforced concrete: mechanical behavior and numerical modeling. ACI Mater J 2010;107(2). March–April.
[33] Denarie E, Habel K, Bruehwiler E. Structural behavior of hybrid elements with advanced cementitious materials (HPFRCC). In: HPRFCC-4. 4th International workshop on high performance fiber reinforced cement composites. Ann Arbor. MI. June 16–18 2003.
[34] Charron JP, Denarie E, Bruehwiler E. Transport properties of water and glycol in an ultra high performance fiber reinforced concrete (UHPFRC) under high tensile deformation. Cem Concr Res 2008;38:689–98.
[35] Cunha VMCF, Barros JAO, Sena-Cruz JM. An integrated approach for modelling the tensile behaviour of steel fiber reinforced self-compacting concrete. Cem Concr Res 2011;41:64–76.
[36] Barragan BE, Gettu R, Martin MA, Zerbino RL. Uniaxial tension test for steel fibre reinforced concrete – a parametric study. Cement Concr Compos 2003;25:767–77.
[37] RILEM TC 162-TDF. Test and design methods for steel fibre reinforced concrete. Uni-axial tension test for steel fibre reinforced concrete. Recommendations. Mater Struct 2011;34(235); 3–6.
[38] Rossi P. High performance multimodal fiber reinforced cement composites (HPMFRCC): the LCPC experience. ACI Mater J 1997;94(6):478–83. November-December.
[39] Naaman AE, Fischer G, Krustulovic-Opara N. Measurement of tensile properties of fiber reinforced concrete: draft submitted to ACI committee 544. In: Reinhardt HW, Naaman AE, editors. Proceedings of rilem international workshop on high performance fiber reinforced cement composites – HPFRCC5, Germany, RILEM Proceedings, Pro. 53, S.A.R.L., Cachan, France, July 2007. p. 3–12.
[40] AASHTO T 132–87. Standard method of test for tensile strength of hydraulic cement mortars. American Association of State and Highway Transportation Officials; 2009. 8 p.
[41] Naaman AE, Wille K. Some correlation between high packing density, ultra-high performance, flow ability, and fiber reinforcement of a concrete matrix. BAC2010 – 2nd Iberian congress on self compacting concrete. university of minho – guimaraes, Portugal; July 1–2 2010.
[42] DAfStB 561: Deutscher ausschuss fuer stahlbeton. Sachstandsbericht – ultrahochfester Beton; 2008. p. 126 [in German].
[43] Wille K. Concrete strength dependent pull-out behavior of deformed steel fibers. In: Electronic proceedings of BEFIB2012 – 8th RILEM international symposium on fibre reinforced, Concrete, Guimaraes, 19–21 September 2012. 12 p.
[44] Wille K, Parra-Montesinos G. Effect of beam size, casting method, and support conditions on flexural behavior of ultra-high-performance fiber-reinforced concrete. ACI Mater J 2012;109(3):379–88. May–June.
[45] Rossi P. Influence of fibre geometry and matrix maturity on the mechanical performance of ultra high-performance cement-based composites. Cement Concr Compos 2013;37:246–8. March.
[46] Naaman AE. High performance fiber reinforced cement composites. In: Shi C, Mo YL, editors. High-performance construction materials. Science and applications; 2008. p. 91–153.
[47] Fantilli AP, Mihashi H, Vallini P. Multiple cracking and strain hardening in fiber-reinforced concrete under uniaxial tension. Cem Concr Res 2009:1217–29.
[48] Doennecke C. Das entfestigungsverhalten ultrahochfester betone (softening behavior of ultra-high strength concretes). Report. University of Leipzig. August 2003. [in German]
[49] Jungwirth J. Zum tragverhalten von zugbeanspruchten bauteilen aus ultra-hochleistungs-faserbeton. Ecole polytechnique federale de Lausanne. Ph.D. thesis. 2006. [in German]
[50] Habel K, Viviani M, Denarie E, Bruehwiler E. Development of the mechanical properties of an ultra-high performance fiber reinforced concrete (UHPFRC). Cem Concr Res 2006(36):1362–70.
[51] Bache NH. 1992. Principles of similitude in design of reinforced brittle matrix composites. In: High performance fiber reinforced cement composites. Rilem proceedings 15; 1992. p. 39–56.